



## ABSTRACT

5  
6 Developing wave packets associated with the extratropical transition (ET) of tropical cy-  
7 clones and winter cyclones in the Western North Pacific (WNP) and Atlantic basins are  
8 diagnosed observationally by compositing reanalysis data over a 32 year period. While the  
9 development of winter cyclones amplifies a weaker wave packet moving through the mid-  
10 latitude storm track, there is no indication of an upstream disturbance during ET; thus,  
11 on average, the wave packet is generated by the ET process. In the WNP, ET and winter  
12 cyclone wave packets have comparable group velocity and amplitude relative to climatology,  
13 whereas ET wave packets have relatively longer wavelength and near-zero group velocity  
14 during the ET process; ET events also have a detectable signal further downstream. Wave  
15 packets associated with winter cyclones in the Atlantic basin have greater amplitude and  
16 have a detectable signal further downstream relative to those associated with ET. Near the  
17 surface, winter cyclones are characterized by larger meridional heat fluxes relative to ET.  
18 WNP ET cyclones are characterized by larger meridional moisture flux convergence and  
19 thus latent heat release relative to their winter counterparts, while Atlantic basin ET and  
20 winter cyclones have similar moisture flux convergence. This result suggests that the wave  
21 packets associated with ET cyclones are related to diabatic processes and could explain why  
22 the amplitude of Atlantic basin ET wave packets are smaller than winter cyclones. Finally,  
23 the greater baroclinicity during winter does not seem to influence the downstream packet  
24 amplitude in either basin.

# 1. Introduction

The extratropical transition (ET) of tropical cyclones (TCs) is often associated with the amplification of an upper-tropospheric anticyclone downstream of the TC (e.g., Jones et al. 2003; Agusti-Panareda et al. 2004; Harr and Dea 2009). The development of this ridge occurs in response to a number of dynamical mechanisms, including the adiabatic interaction of the TC circulation with the midlatitude waveguide (e.g., Ferreira and Schubert 1999; Riemer et al. 2008), and the diabatic outflow from either the TC or the baroclinic zone that often develops on the down-shear side of the cyclone (e.g., Bosart and Dean 1991; Harr and Elsberry 2000; Riemer et al. 2008; Riemer and Jones 2010; Torn 2010). The development of this downstream ridge serves as an impulsive disturbance on the midlatitude flow, which can give rise to wave packets and downstream development (e.g., Simmons and Hoskins 1979; Chang and Orlanski 1993; Orlanski and Sheldon 1995; Hakim 2003), spreading the impact of the ET event further downstream from the cyclone itself.

Previous studies have found that the downstream response of the midlatitudes to ET varies from case to case, depending on the phasing of the TC with midlatitude features, and that downstream development does not require a reintensifying tropical cyclone (e.g., Harr and Dea 2009; Riemer and Jones 2010). These wave packets are often associated with forecast errors well downstream of the ET (e.g., Jones et al. 2003; Harr et al. 2008; Anwender et al. 2008). Consequently, this motivates a deeper understanding of the development and propagation of these wave packets over many cases.

ET events are not the only phenomenon that can create impulsive wave packets within the midlatitude flow. Much of the literature on this topic has focused on the role of midlatitude cyclones. Both observational (e.g., Orlanski and Katzfey 1991; Chang 2000; Hakim 2003) and statistical (e.g., Chang 1993, 1999; Chang and Yu 1999) studies suggest that these wave packets are energy sources whereby upstream disturbances seed downstream disturbances. Moreover, midlatitude forecast errors develop and propagate similarly to wave packets (e.g., Hakim 2005). For example, forecasts have also been shown to be sensitive to

52 wave packet initialization (e.g., Langland et al. 2002) and that the impact of assimilating  
53 targeted observations spreads downstream as a wave packet (e.g., Szunyogh et al. 2000).

54 The goal of this work is to compare wave packets associated with ET with those asso-  
55 ciated with winter cyclones in the Western North Pacific (WNP) and Atlantic basins. In  
56 particular, this study evaluates whether one can reject the null hypothesis that there is no  
57 meaningful difference in the genesis, structure, and propagation of wave packets associated  
58 with ET and winter cyclones. This hypothesis is tested by comparing a large sample of wave  
59 packets associated with ET and winter cyclones by averaging over many cases and applying  
60 the packet diagnostic technique outlined in Hakim (2003) to quantitatively compare packet  
61 properties. While previous work on the downstream impact of ET has focused on individual  
62 case studies or a small number of cases, this study bridges the ET and wintertime wave  
63 packet literature for a large sample.

64 The remainder of the paper proceeds as follows. Section 2 describes the dataset and  
65 methods used to compute the wave packets and their properties. Results of the calculations  
66 are presented in section 3 followed by a summary and conclusions in section 4.

## 67 **2. Method**

68 Wave packets associated with ET and winter storms in the Western North Pacific (WNP)  
69 and Atlantic basins are evaluated by compositing atmospheric fields, similar to the strategy  
70 employed by Hakim (2003). These two basins are chosen because of the overlap between the  
71 region of maximum ET and winter cyclogenesis frequency (e.g., Sanders and Gyakum 1980;  
72 Klein et al. 2000; Hart and Evans 2001) and the numerous studies of ET in each basin.

73 Atmospheric fields are taken from version 1 of the National Centers for Environmental  
74 Prediction (NCEP) Climate Forecast System (CFS) Reanalysis dataset (Saha et al. 2010)  
75 on mandatory constant pressure surfaces, with horizontal and temporal resolution of  $2.5^\circ$

76 and 6 h, respectively, from 1979-2010<sup>1</sup>. Anomalies are defined as deviations from a moving-  
77 average climatology, meaning that every day of the year has a unique climatology, which  
78 is defined as the average of all daily fields within  $\pm 14$  d of the day of interest during the  
79 32 year period. This method of computing the climatology has the advantage of producing a  
80 smooth climatology from one day to the next. Statistically significant anomalies are defined  
81 in terms of a two-side Student’s t test with a threshold of 95%.

82 The sample of winter cyclone wave packets is determined by identifying rapidly deepening  
83 cyclones at the location of highest frequency in each basin. As in Hakim (2003), baroclinic  
84 cyclones are defined as local maxima in 1000 hPa geostrophic relative vorticity exceeding  
85  $10^{-4} \text{ s}^{-1}$  during November–March. Several additional checks are employed to ensure that  
86 individual cyclone events are identified. Any cyclone that is within  $25^\circ$  of another cyclone is  
87 removed from consideration. To ensure that the same event is not identified twice, any cy-  
88 clone within  $15^\circ$  latitude and longitude of a previously identified cyclone during the previous  
89 24 h is removed from the list of potential candidates. Hereafter, “ $t = 0$ ” refers to the time  
90 when the cyclone exceeds the above critical value, which approximates when the cyclone  
91 reaches the mature stage. Based on these criteria, the maximum number of cyclone events  
92 in the WNP occurs within  $35^\circ\text{N}$ - $40^\circ\text{N}$ ,  $145^\circ\text{E}$ - $155^\circ\text{E}$ , while in the Atlantic the maximum  
93 number occurs within  $40^\circ\text{N}$ - $45^\circ\text{N}$ ,  $55^\circ\text{W}$ - $65^\circ\text{W}$ ; the latter region is slightly to the east of the  
94 box used in Hakim (2003). These boxes contain 281 and 334 cases in the WNP and Atlantic  
95 Basins, respectively.

96 Wave packets for ET cases are determined by evaluating all TCs contained in the Joint  
97 Typhoon Warning Center (JTWC) WNP best track data and the National Hurricane Center  
98 (NHC) Atlantic data from 1979-2010. A TC is considered a candidate for ET if the track

---

<sup>1</sup>Although the raw resolution of the CFS reanalysis is  $0.5^\circ$ , at this resolution, the mass fields are noisy near TC, likely due to the method used to relocate the TC from its location in the 6 h forecast to the observed position in the analysis (e.g., Liu et al. 2000); therefore, the lower resolution  $2.5^\circ$  dataset, which shows no evidence of this issue, is employed. Given that this study mainly focuses on synoptic-to-planetary scale features, this choice of resolution should not be a limitation

99 underwent recurvature at some point in its life, meaning it had an easterly component of  
100 motion, and the TC moved poleward of  $20^{\circ}\text{N}$ ; the latter condition removed any TCs that  
101 drifted within the deep tropics, but never moved into the midlatitudes. For each of the  
102 remaining TCs, the reanalysis position is determined by finding the minimum in 1000 hPa  
103 geopotential height each 6 h; for a majority of times, the best track and reanalysis positions  
104 are within  $1^{\circ}$  of each other. At each time, the asymmetry parameter from the Hart (2003)  
105 cyclone phase space is calculated from reanalysis data. This parameter provides a measure of  
106 the thermal asymmetry across the cyclone and has been used to objectively identify the onset  
107 of transition. As in Hart (2003), the onset of transition is defined as when the asymmetry  
108 parameter exceeds 10 m and is hereafter referred to as “ $t = 0$ ”. In each basin, the maximum  
109 number of ET cases within any  $5^{\circ} \times 10^{\circ}$  box is 34, which does not provide a robust composite  
110 to calculate wave packet properties due to the small number of cases. Instead, this study  
111 considers all cases where the onset of ET occurs between  $30^{\circ}\text{-}35^{\circ}\text{N}$  and  $120^{\circ}\text{-}180^{\circ}\text{E}$  in the  
112 WNP and  $35^{\circ}\text{-}40^{\circ}\text{N}$  and  $90^{\circ}\text{-}30^{\circ}\text{W}$  in the Atlantic; these latitude bands contain the largest  
113 number of ET onset within each basin. This choice results in 112 and 91 cases in the WNP  
114 and Atlantic, respectively. It is worth noting that this study considers all cases of ET within  
115 this location, regardless of whether the TC underwent baroclinic reintensification. Previous  
116 studies have suggested that the completion of ET is not necessary for a midlatitude response  
117 to occur (e.g., Harr and Dea 2009; Riemer and Jones 2010).

118 Figure 1 shows the number of ET and winter cyclones in each basin as a function of  
119 month. While the largest number of ET cases occur in September and October, the winter  
120 cases are mainly in February and March in the WNP and December-January in the Atlantic.  
121 The difference in timing between ET and winter cyclones results in different background  
122 states through which the wave packets develop and propagate; the implications of which are  
123 explored in greater detail in the next section.

124 *a. Wave-packet analysis*

125 The remainder of this paper will employ ensemble averaging of ET and baroclinic cyclone  
126 cases in each basin over a range of time lags. The relatively large number of baroclinic cyclone  
127 cases allow for straightforward averaging in an Earth-relative frame of reference; however, for  
128 the ET cases, all fields are shifted to a common longitude, which is defined as the longitude  
129 of the cyclone at the onset of ET. As pointed out in Hakim (2003), the ensemble averaging  
130 method has the advantage that it is relatively simple and does not integrate away time and  
131 amplitude information; however, the signal contained in the ensemble mean will degrade to  
132 zero for nonzero time lags due to different trajectories and velocities of individual events.

133 Properties of the wave packet at each time are analyzed using the methods outlined  
134 in Hakim (2003) and are summarized here. Wave packets are identified from the 300 hPa  
135 meridional wind field over a  $250^\circ$  longitude window centered on the maximum in the absolute  
136 value at a grid point. The peak of the packet is determined by fitting a polynomial to the  
137 six grid point extrema about the maximum value, while the local extrema and zero crossings  
138 are determined from the interpolated polynomial near the packet peak. The leading edge of  
139 the packet is determined by linear regression of the interpolated packet to an exponential  
140 profile, with the leading edge defined as 2.5  $e$ -folding distance from the peak (8% of the  
141 peak value). Finally, the wavelength of the packet is determined by computing the distance  
142 between zero crossings and extrema.

### 143 **3. Results**

144 *a. Western Pacific*

145 Composites of the 300 hPa meridional wind during WNP ET and winter cyclone cases  
146 reveal important differences in the wave packet evolution prior to  $t=0$ . (Fig. 2). The domi-  
147 nant signal in the ET wave packet at  $-48$  h is a  $3 \text{ m s}^{-1}$  wind couplet centered near  $155^\circ\text{E}$

148 with associated weak ridging in the PV field<sup>2</sup> (Fig. 2a). By  $-24$  h, the amplitude of the  
149 meridional wind increases to  $9 \text{ m s}^{-1}$ , with the corresponding undulation in the PV field  
150 suggestive of an amplifying ridge  $5^\circ$  to the east of the  $-48$  h position (Fig. 2c). At the onset  
151 of transition ( $0$  h), the ridge amplitude increases further; however, the axis of this ridge has  
152 only moved  $5^\circ$  relative to the  $-24$  h position (Fig. 2e). Moreover, there is an indication of  
153 a downstream trough at  $170^\circ\text{W}$ , suggesting a nascent wave packet has developed. Overall,  
154 this result suggests that the process of ET produces an amplifying, but nearly stationary  
155 ridge, with little evidence of an upstream precursor disturbance. This result differs from  
156 Archambault et al. (2012) who showed that recurving cyclones are preceded by an upstream  
157 trough moving through the midlatitude flow. The difference between these two studies is  
158 likely due to how each study defines the lag time. Archambault et al. (2012) defined  $t=0$  to  
159 be the time when the TC reaches its westernmost position, while this study defines  $t=0$  to  
160 be the onset of transition; these two times can differ by 0-3 days depending on the case.

161 In contrast to ET cases, the winter cyclone composite is characterized by a predecessor  
162 wave packet prior to  $t=0$ . At  $t=-48$  h, there is a relatively weak ( $3 \text{ m s}^{-1}$ ) wave packet  
163 centered on Japan that subsequently amplifies as it moves eastward with time (Fig. 2b).  
164 Over the next 48 h, the meridional wind anomalies increase to  $18 \text{ m s}^{-1}$  during which time  
165 the packet moves  $30^\circ$  to the east (Fig. 2d,f). Similar to Hakim (2003), this pattern suggests  
166 that the winter cyclones tend to amplify a weak pre-existing wave packet that is moving  
167 through the midlatitude wave guide.

168 In addition to differences in how wave packets are generated during ET and winter  
169 cyclones, there are also subtle differences in how the packets evolve after  $t=0$ . For the  
170 ET cyclones, the wave packet is associated with an amplifying trough at  $160^\circ\text{W}$  at 24 h  
171 (Fig. 2g) and finally a nascent ridge with the axis over the west coast of the United States  
172 by 72 h (Fig. 2i,k) before vanishing over North America by 96 h (not shown). Although the

---

<sup>2</sup>To facilitate comparison with the winter cyclone cases, the geography on the ET figures is oriented such that the cyclone position at  $t=0$  matches the winter cyclone position at  $t=0$

173 winter cyclone wave packet exhibits a similar eastward propagation, the southern edge of  
174 the packet is characterized by refraction into the tropics starting at 24 h (Fig. 2h), which is  
175 not present in the ET composites. Moreover, it appears that the winter cyclone wave packet  
176 peak does not reach North America, while it does in the ET cyclones, which suggests that  
177 on average ET cyclone wave packets propagate further east in the WNP. This difference is at  
178 least partly due to the nature of the waveguide associated with these two types of systems.  
179 The ensemble-mean meridional PV gradient in the ET cyclones is nearly constant across  
180 the entire Pacific Ocean, which implies a zonally consistent waveguide. By contrast, the  
181 winter cases are characterized by a higher meridional PV gradient to the west of the dateline  
182 compared to the east. We hypothesize that the greater zonal variation in the meridional PV  
183 gradient contributes to a greater range of group speeds for the winter cyclone cases, which  
184 blurs the sample-average signal.

185 The ET and winter cyclone wave packet properties are objectively analyzed using the  
186 methods outlined in section 2b to determine their wavelength, amplitude and group velocity.  
187 Figure 3a,b shows the wave packets associated with ET and winter cyclones at  $t=0$ ; these  
188 figures are similar to what is obtained at  $t=-24 - +48$  h (not shown). For both ET and winter  
189 cases, the wave packets look similar to those observed in Hakim (2003). In particular, the  
190 wave packet amplitude exhibits a good fit to an exponential profile with an abrupt westerly  
191 edge, consistent with impulsive disturbances, which have an exponential zonal structure  
192 (e.g., Swanson and Pierrehumbert 1994).

193 Comparing the packet peak amplitude confirms many of the aforementioned ideas of the  
194 development and propagation of ET and winter cyclone wave packets. The ET packet peak  
195 amplitude increases from  $10 \text{ m s}^{-1}$  at  $-24$  h to  $17 \text{ m s}^{-1}$  12 h after the onset of ET, then  
196 decreases to  $10 \text{ m s}^{-1}$  by 48 h (Fig. 4a). By contrast, the winter packet amplitude is  $3 \text{ m s}^{-1}$   
197 higher than the ET wave packet at  $-24$  h, peaks at  $18.5 \text{ m s}^{-1}$  at 0 h, and decreases at a  
198 slower rate relative to the ET packet. While this result implies that winter cyclone wave  
199 packets have greater amplitude than ET wave packets, this is potentially deceiving because

200 the climatological standard deviation in meridional wind is larger during the winter cyclones  
201 times (primarily February-March) compared to when ET occurs (September-October). To  
202 address this concern, the packet peak amplitude for each case is normalized by the climato-  
203 logical standard deviation in the 300 hPa meridional winds at the location of the packet peak  
204 for that day. Between  $-24$  h and  $+24$  h, the ET and winter cyclone normalized packet am-  
205 plitudes are within 0.04 normalized units of one another; thereafter, ET and winter cyclone  
206 wave packets are of equal amplitude relative to climatology.

207 The group velocity calculations support the notion that the development of winter cy-  
208 clones results in the enhancement of an existing wave packet, while ET leads to the generation  
209 of a new packet. Fig. 5 shows that the winter cyclone wave packet group velocity increases  
210 from  $6 \text{ m s}^{-1}$  at  $t=-24$  h to a maximum of  $26 \text{ m s}^{-1}$  at 6 h, which is slower than the back-  
211 ground flow of  $40 \text{ m s}^{-1}$ . The reduction in group velocity with time beyond 6 h likely reflects  
212 the decrease in the background flow across the basin, which could act to focus wave packets  
213 (e.g., Esler and Haynes 1999; Chang and Yu 1999; Hakim 2003). By contrast, the ET wave  
214 packet group velocity is either negative or zero until  $t=0$ , implying a nearly stationary wave  
215 packet during which time the amplitude is increasing (c.f., Fig. 4a). This result suggests that  
216 external forcing, such as latent heat release associated with the transitioning TC is critical  
217 and that the forcing has near zero or negative zonal velocity. Beyond 0 h, the group velocity  
218 increases to  $15 \text{ m s}^{-1}$ , except for the large spike at 24 h, which could be an artifact of the  
219 limited number of ET cases used in this compositing technique.

220 Figure 6 shows the packet peak wavelength for both the ET and winter cyclone cases. As  
221 suggested by Fig. 2, the ET wave packet has a wavelength that is 500-700 km longer than  
222 the winter cyclone cases at all lead times. These wavelength differences are likely due to the  
223 structure of the background flow through which the wave packets are traveling.

224 The different behavior of the ET and winter wave packets prior to 0 h suggests that  
225 different dynamical processes may be responsible for the generation and amplification of the  
226 wave packets. As stated earlier, both adiabatic and diabatic processes can contribute to

227 the amplification of the midlatitude flow. To investigate this possibility, ensemble-average  
228 lower tropospheric meridional temperature and moisture fluxes are computed at  $t=0$  (other  
229 times are qualitatively similar) for both ET and winter cyclones. Fig. 7 shows the 900 hPa  
230 meridional heat flux, which is computed by multiplying the meridional wind deviation from  
231 climatology by the temperature deviation from climatology at each grid point. For both  
232 ET and winter cyclones, there is a maximum in meridional heat flux on the eastern side of  
233 the cyclone within the region of southerly geostrophic winds as implied by the geopotential  
234 height contours. Although the location of positive heat flux is similar in both sets of  
235 cases, the maximum in the winter cyclone heat flux is roughly twice the value of the ET  
236 cyclone. Moreover, the winter cyclones are also characterized by a greater spatial coverage  
237 of heat flux greater than  $8 \text{ K m s}^{-1}$ . Assuming that the largest temperature gradients are  
238 near the surface, this result suggests that, relative to ET cyclones, the winter cyclones are  
239 characterized by greater forcing for height rises and thus upper tropospheric ridge building  
240 via the quasi-geostrophic height tendency equation. Larger meridional heat fluxes might be  
241 expected for the winter cyclones given the enhanced climatological meridional temperature  
242 gradient during winter (not shown).

243 Whereas winter cyclones are characterized by larger meridional heat fluxes, the opposite  
244 is true for moisture fluxes at the same level (Fig. 8a,b). Here, moisture fluxes are computed  
245 in the same manner as heat fluxes, except that temperature perturbations are replaced by  
246 water-vapor mixing ratio deviations from climatology. Although the positive moisture flux  
247 area is similar in both cases, the maximum flux in the ET cases is  $45 \text{ g kg}^{-1} \text{ m s}^{-1}$ , compared  
248 to  $27 \text{ g kg}^{-1} \text{ m s}^{-1}$  in the winter cyclones, suggesting that the ET cyclones are characterized  
249 by larger poleward moisture transport. Moreover, the ET cases are characterized by a  
250 maximum moisture flux convergence of  $6.0 \times 10^{-5} \text{ g kg}^{-1} \text{ s}^{-1}$  on the poleward side of the  
251 moisture flux maximum, compared to  $2.5 \times 10^{-5} \text{ g kg}^{-1} \text{ s}^{-1}$  in the winter cyclone. These  
252 differences imply that ET cases are characterized by greater latent heat release and forcing  
253 for height rises compared to winter cyclones. This result agrees with the idealized simulations

254 of Riemer and Jones (2010), who show that the initial downstream response to ET is mainly  
255 due to diabatic processes.

256 *b. Atlantic*

257 Composites of Atlantic basin ET and winter cyclone wave packets show many qualitative  
258 similarities to their western Pacific counterparts, with smaller ET amplitude. Figure 9  
259 indicates that Atlantic ET is characterized by a nearly stationary amplifying ridge prior to  
260 the onset of ET, similar to WNP ET. In addition, there is a northerly wind signal that  
261 moves from western North America at  $-48$  h to just upstream of the developing ridge at  
262 0 h. By comparison, the winter cyclones are characterized by a weaker pre-existing wave  
263 packet located at  $100^\circ\text{W}$  at  $-48$  h that subsequently moves east and amplifies with time  
264 (Fig. 9b,d,f).

265 Following the onset of ET, the wave packet moves eastward toward Europe; however,  
266 the statistically significant signal quickly decays, such that beyond 48 h, there is no signal  
267 in the 300 hPa meridional wind field. By contrast, the winter cyclone wave packet has a  
268 statistically significant signal that reaches Europe by 48 h and exhibits refraction into the  
269 tropics (Fig. 9h,j). Overall, these results suggest that, on average, ET wave packets have  
270 difficulty maintaining their amplitude as they move across the Atlantic Ocean relative to  
271 those associated with winter cyclones.

272 ET and winter cyclone wave packet properties are also computed within this basin. For  
273 winter cyclones, the peak packet amplitude is  $21 \text{ m s}^{-1}$  at 0 h, then decays to half that value  
274 by 42 h when the packet reaches Europe, while the ET packet amplitude has a maximum  
275 value of  $15 \text{ m s}^{-1}$  before decreasing to less than  $10 \text{ m s}^{-1}$  by 36 h (Fig. 4b). Normalizing  
276 the amplitude by the climatological standard deviation indicates that the ET wave packet  
277 amplitude is about 10% less than winter cyclones.

278 Wave packet group velocities are consistent with the WNP results, which showed that  
279 winter cyclones enhance an existing wave packet, whereas ET packets are produced in situ

280 (Fig. 5b). The winter-cyclone wave packets have a group velocity that varies between 15–  
281  $30 \text{ m s}^{-1}$  throughout the period. By contrast, as was observed in the WNP cases, the ET wave  
282 packet group velocity is slightly negative until 0 h, which is likely related to the combination  
283 of the aforementioned midlatitude disturbance getting closer to the ridge associated with  
284 ET and the slow zonal motion of the forcing. Beyond that time, the ET packet peak group  
285 velocity is quite similar to the winter cyclones, suggesting its propagation properties are  
286 similar once the packet is of sufficient amplitude and detached from the forcing. Finally,  
287 the ET packet wavelength is greater than the winter cyclones for most times prior to 0 h,  
288 though they are quite similar thereafter (Fig. 6b).

289 In the lower troposphere, Atlantic basin winter cyclones have similar meridional heat  
290 fluxes relative to their western Pacific counterparts, while the Atlantic ET cyclones are char-  
291 acterized by smaller values compared to WNP ET. Although the spatial coverage of positive  
292 heat fluxes in the WNP and Atlantic ET composites are fairly similar, the maximum value  
293 in the Atlantic basin ( $20 \text{ K m s}^{-1}$ ) is 25% smaller than the western Pacific (cf., Fig. 7a,c).  
294 By contrast, the winter cyclones in both basins have similar areas of positive heat flux and  
295 maximum values (Fig. 7b,d); therefore, it appears that while the forcing for height rises  
296 in winter cyclones are similar in the two basins, the same is not true for ET. The lower  
297 heat fluxes for Atlantic ET would be expected to produce less forcing for height rises in the  
298 downstream ridge relative to WNP ET.

299 In addition to having weaker meridional heat fluxes, Atlantic ET cases also appears to  
300 have weaker moisture fluxes relative to the WNP cases (Fig. 8c-d). The maximum moisture  
301 flux in the Atlantic ET cases is  $31 \text{ g kg m s}^{-1}$ , compared to  $29 \text{ g kg m s}^{-1}$  for Atlantic winter  
302 cyclones and  $45 \text{ g kg m s}^{-1}$  for WNP ET. This result suggests that, on average, Atlantic ET  
303 cases have smaller forcing for height rises due to diabatic heating, which could explain why  
304 the amplitude of ET wave packets in the Atlantic is smaller than winter cyclones.

305 Another reason for the lower amplitude in Atlantic ET wave packets vs. winter cyclones  
306 could be due to the case-selection criteria. Recall that the Atlantic composite includes all

307 TCs that underwent ET between 35°N and 40°N. For some of these cases, this happened  
308 while the TC was over land. By contrast, none of the WNP ET cases made landfall over an  
309 appreciable land mass, except for Japan. To determine whether these over-land ET cases  
310 bias the ensemble-mean ET wave packet, the composite calculations are repeated for all ET  
311 cases that remained over water prior to and during ET. The ensemble-mean wave packet for  
312 the over-water Atlantic ET cases is nearly identical to the ensemble-mean wave packet for  
313 all (not shown); therefore, land does not appear to be a factor in Atlantic ET having weaker  
314 wave packets.

315 Another possible factor for the difference in ET and winter cyclone wave packets is that  
316 ET is most frequent in August, September and October (ASO) when the background state  
317 could be less favorable for high-amplitude, long-lasting wave packets. The role of the seasonal  
318 cycle is tested by computing wave packet statistics for non-TC Atlantic cyclones that meet  
319 the cyclone criteria described in section 2 between 35°–40°N and 90°–30°W during ASO using  
320 the longitude-shifting procedure employed for ET cyclones. Wave packets associated with  
321 ASO cyclones have a group velocity of 10–12 m s<sup>-1</sup>, a wavelength of 3000 km, and packet peak  
322 amplitude of 24 m s<sup>-1</sup> (normalized amplitude of 1.4 times climatology; not shown). These  
323 properties bear greater resemblance to winter cyclones relative to ET; therefore, it appears  
324 that the difference in Atlantic ET and winter cyclone wave packets cannot be attributed to  
325 the seasonal cycle alone.

## 326 4. Summary and Conclusions

327 This study poses the hypothesis that wave packets associated with the extratropical  
328 transition of tropical cyclones in the western Pacific and Atlantic basins are on average  
329 quantitatively indistinguishable from those associated with winter cyclones. This hypothesis  
330 is tested by computing ensemble averages of ET and winter cyclone cases from reanalysis  
331 data over a 32 yr period. The properties of the wave packet are then analyzed using the

332 techniques described in Hakim (2003).

333 For both the western Pacific and Atlantic basins, the wave packets associated with ET  
334 and winter cyclones exhibit many similarities, with the most significant differences apparent  
335 in the genesis and decay of the packet. Prior to the onset of ET, there is little evidence of an  
336 upstream wave packet in either the WNP or Atlantic basins. Instead, the development of the  
337 downstream ridge associated with ET appears to produce a wave packet in situ, which then  
338 propagates eastward once it escapes tropical forcing. By contrast, winter cyclone genesis  
339 appears to amplify a pre-existing wave packet that can be tracked backward in time through  
340 the midlatitude storm track. As a consequence, it is possible to reject the null hypothesis  
341 that there is no meaningful difference in the genesis of ET and winter wave packets.

342 Following the onset of ET and winter cyclone maturity, the wave packets exhibit simi-  
343 lar characteristics of downstream propagation and eventual dissipation. In both basins, the  
344 group velocity and, to a lesser extent, the wavelength, are quantitatively similar, suggesting  
345 that once a packet matures, the behavior is similar in both cases. While WNP ET and  
346 winter cyclone wave packets have similar amplitudes relative to climatology, the amplitude  
347 of Atlantic winter cyclone packets is greater than ET. In addition, while WNP ET packets  
348 have a statistically significant signal that propagates further downstream relative to winter  
349 cyclones, the opposite is true in the Atlantic basin. These results suggest that wave pack-  
350 ets associated with WNP ET and winter cyclones have similar structure and propagation  
351 characteristics, thus it is difficult to reject the null hypothesis that there is any meaningful  
352 difference. By contrast, Atlantic winter cyclone wave packets are strong and longer-lived  
353 than their ET counterpart, thus there are meaningful differences in this basin.

354 Some of the differences between ET and winter cyclone wave packets are likely related to  
355 the dynamics of packet development. In both the Atlantic and western Pacific basins, winter  
356 cases are characterized by larger tropospheric meridional temperature fluxes relative to ET  
357 cyclones, implying that winter cyclones have greater adiabatic forcing for geopotential height  
358 rises and thus wave packet amplification. On the other hand, WNP ET cases have larger

359 lower tropospheric meridional moisture fluxes and flux convergence relative to the winter  
360 cases. Assuming that moisture flux convergence correlates with latent heat release implies  
361 that diabatic processes are more important in wave packet amplification in ET relative to  
362 winter cyclones. In the Atlantic basin, the moisture fluxes during ET are comparable to  
363 winter cyclones and smaller than WNP ET, suggesting relatively smaller forcing for height  
364 rises and wave packet amplification, which could explain why Atlantic-basin ET wave packets  
365 are on average weaker than winter cyclones.

366 Although this work indicates that ET and winter cyclone wave packets have many similar  
367 characteristics, the differences in how these packets are produced could have important  
368 consequences on downstream predictability during each event. Given the relative dearth of  
369 in situ moisture observations over the lower-tropospheric ocean, models may have relatively  
370 large moisture analysis errors, which could translate into different latent heating rates and  
371 details in the downstream ridge amplitude during ET cases (e.g., Torn 2010). Moreover,  
372 since the packet is produced by the ET cyclone itself, TC track errors could also introduce  
373 uncertainty in the timing and amplitude of the subsequent wave packet (e.g., Harr et al.  
374 2008; Anwender et al. 2008; Riemer and Jones 2010). By comparison, the winter cyclones  
375 appear to amplify pre-existing wave packets; therefore, provided the upstream disturbance  
376 is resolved by the current observation network, downstream predictability might not be as  
377 sensitive to details of winter cyclogenesis. Future work will evaluate the aforementioned  
378 hypothesis by comparing forecasts during ET events with those of winter cyclones.

379 *Acknowledgments.*

380 This research benefited from discussions with Heather Archambault, Lance Bosart and  
381 Jack Beven. CFSR data was obtained from the National Oceanic and Atmospheric Ad-  
382 ministration National Climatic Data Center. This work was sponsored by NSF Grants  
383 AGS-084809, and AGS-0842384.

## REFERENCES

- 386 Agusti-Panareda, A., C. D. Thorncroft, G. C. Craig, and S. L. Gray, 2004: The extratropical  
387 transition of hurricane Irene (1999): A potential-vorticity perspective. *Quart. J. Roy. Met.*  
388 *Soc.*, **130**, 1047–1074.
- 389 Anwender, D., P. A. Harr, and S. C. Jones, 2008: Predictability associated with the down-  
390 stream impacts of the extratropical transition of tropical cyclones: Case studies. *Mon.*  
391 *Wea. Rev.*, **136**, 3226–3247.
- 392 Archambault, H. M., D. Keyser, and L. F. Bosart, 2012: A compositing study of the down-  
393 stream flow response to recurving tropical cyclones in the western north pacific. *Mon. Wea.*  
394 *Rev.*, Submitted.
- 395 Bosart, L. F. and D. B. Dean, 1991: The agnes rainstorm of June 1972: Surface feature  
396 evolution culminating in inland storm redevelopment. *Wea. Forecasting*, **6**, 515–537.
- 397 Chang, E. K. M., 1993: Downstream development of baroclinic waves as inferred from  
398 regression analysis. *J. Atmos. Sci.*, **50**, 2038–2053.
- 399 Chang, E. K. M., 1999: Characteristics of wave packets in the upper troposphere. Part II:  
400 Seasonal and hemispheric variations. *J. Atmos. Sci.*, **56**, 1729–1747.
- 401 Chang, E. K. M., 2000: Wave packets and life cycles of troughs in the upper troposphere:  
402 Examples from the Southern Hemisphere summer season of 1984/85. *Mon. Wea. Rev.*,  
403 **128**, 28–50.
- 404 Chang, E. K. M. and I. Orlanski, 1993: On the dynamics of a storm track. *J. Atmos. Sci.*,  
405 **50**, 999–1015.

- 406 Chang, E. K. M. and D. B. Yu, 1999: Characteristics of wave packets in the upper tropo-  
407 sphere. Part I: Northern Hemisphere winter. *J. Atmos. Sci.*, **56**, 1708–1728.
- 408 Esler, J. G. and P. H. Haynes, 1999: Mechanisms for wave packet formation and maintenance  
409 in a quasigeostrophic two-layer model. *J. Atmos. Sci.*, **56**, 2457–2490.
- 410 Ferreira, R. N. and W. H. Schubert, 1999: The role of tropical cyclones in the formation of  
411 tropical upper-tropospheric troughs. *J. Atmos. Sci.*, **56**, 2891–2907.
- 412 Hakim, G. J., 2003: Developing wave packets in the North Pacific storm track. *Mon. Wea.*  
413 *Rev.*, **131**, 2824–2837.
- 414 Hakim, G. J., 2005: Vertical structure of midlatitude analysis and forecast errors. *Mon.*  
415 *Wea. Rev.*, **133**, 567–578.
- 416 Harr, P. A., D. Anwender, and S. C. Jones, 2008: Predictability associated with the down-  
417 stream impacts of the extratropical transition of tropical cyclones: Methodology and a  
418 case study of Typhoon Nabi (2005). *Mon. Wea. Rev.*, **128**, 2613–2633.
- 419 Harr, P. A. and J. M. Dea, 2009: Downstream development associated with the extratropical  
420 transition of tropical cyclones over the Western North Pacific. *Mon. Wea. Rev.*, **137**, 1295–  
421 1319.
- 422 Harr, P. A. and R. L. Elsberry, 2000: Extratropical transition of tropical cyclones over the  
423 western north Pacific. Part I: Evolution of structural characteristics during the transition  
424 process. *Mon. Wea. Rev.*, **128**, 2613–2633.
- 425 Hart, R. E., 2003: A cyclone phase space derived from thermal wind and thermal asymmetry.  
426 *Mon. Wea. Rev.*, **131**, 585–616.
- 427 Hart, R. E. and J. L. Evans, 2001: A climatology of the extratropical transition of Atlantic  
428 tropical cyclones. *J. Climate*, **14**, 546–564.

429 Jones, S. C., et al., 2003: The extratropical transition of tropical cyclones: Forecast chal-  
430 lenges, current understanding, and future directions. *Wea. Forecasting*, **18**, 1052–1092.

431 Klein, P. M., P. A. Harr, and R. L. Elsberry, 2000: Extratropical transition of western North  
432 Pacific tropical cyclones: An overview and conceptual model of the transformation stage.  
433 *Wea. Forecasting*, **15**, 373–395.

434 Langland, R. H., M. A. Shapiro, and R. Gelaro, 2002: Initial condition sensitivity and error  
435 growth in forecasts of the 25 January 2000 east coast snowstorm. *Mon. Wea. Rev.*, **130**,  
436 957–974.

437 Liu, Q., T. Marchok, H.-L. Pan, M. Bender, and S. J. Lord, 2000: Improvements in hurricane  
438 initialization and forecasting at NCEP with global and regional (GFDL) models. Tech.  
439 rep., NOAA Tech. Procedures Bull. 472, 7 pp., Camp Springs, MD.

440 Orlandi, I. and J. J. Katzfey, 1991: The life cycle of a cyclone wave in the southern hemi-  
441 sphere. Part I: Eddy energy budget. *J. Atmos. Sci.*, **48**, 1972–1998.

442 Orlandi, I. and J. P. Sheldon, 1995: Stages in the energetics of baroclinic systems. *Tellus*,  
443 **47**, 606–628.

444 Riemer, M. and S. C. Jones, 2010: The downstream impact of tropical cyclones on a de-  
445 veloping baroclinic wave in idealized scenerios of extratropical transition. *Quart. J. Roy.*  
446 *Met. Soc.*, **136**, 617–637.

447 Riemer, M., S. C. Jones, and C. A. Davis, 2008: The impact of extratropical transition on  
448 the downstream flow: An idealized modelling study with a straight jet. *Quart. J. Roy.*  
449 *Met. Soc.*, **134**, 69–91.

450 Saha, S., et al., 2010: The NCEP Climate Forecast System Reanalysis. *Bull. Amer. Meteor.*  
451 *Soc.*, **91**, 1015–1057.

- 452 Sanders, F. and J. R. Gyakum, 1980: Synoptic-dynamic climatology of the “Bomb”. *Mon.*  
453 *Wea. Rev.*, **108**, 1589–1606.
- 454 Simmons, A. J. and B. J. Hoskins, 1979: Downstream and upstream development of unstable  
455 baroclinic waves. *J. Atmos. Sci.*, **36**, 1239–1254.
- 456 Swanson, K. and R. T. Pierrehumbert, 1994: Nonlinear wave packet evolution on a baro-  
457 clinically unstable jet. *J. Atmos. Sci.*, **51**, 384–396.
- 458 Szunyogh, I., Z. Toth, R. E. Morss, S. J. Majumdar, B. J. Etherton, and B. C. H., 2000:  
459 The effect of targeted dropsonde observations during the 1999 winter storm reconnaissance  
460 program. *Mon. Wea. Rev.*, **128**, 3520–3537.
- 461 Torn, R. D., 2010: Diagnosing the factors that influence downstream ridging during extrat-  
462 ropical transition. *J. Atmos. Sci.*, **67**, 817–833.

## 463 List of Figures

- 464 1 Number of winter baroclinic cyclone (black) and extratropical transition cases  
465 (gray) in the (a) western Pacific and (b) Atlantic basin used in this study as  
466 a function of month. 22
- 467 2 Ensemble-mean time evolution of the Western Pacific extratropical transition  
468 (left column) and winter cyclone (right column) wave packets at 300 hPa. The  
469 heavy lines denote the meridional wind every  $3 \text{ m s}^{-1}$ , with dashed indicating  
470 negative values, with the zero contour removed. In the left (right) columns,  
471 the thin lines denote the 330 K potential vorticity between 3-5 (1-3) PVU [ $1$   
472  $\text{PVU} = 10^{-6} \text{ m}^2 \text{ K} (\text{kg s})^{-1}$ ] each 1 PVU. The underlying map in the left  
473 column is oriented such that the composite center longitude at  $t=0$  matches  
474 the winter cyclone box longitude. 23
- 475 3 Western Pacific (a) ET and (b) winter cyclone wave-packet analysis at  $t=0$ .  
476 Solid lines denote the anomaly meridional wind ( $\text{m s}^{-1}$ ) as a function of lon-  
477 gitude, while the dashed lines are a linear fit to an exponential profile from  
478 the packet peak to 2.5  $e$ -folding distances from the peak. (c) and (d) as in (a)  
479 and (b) but for Atlantic wave packets. 24
- 480 4 Amplitude ( $\text{m s}^{-1}$ ) of the ET (solid) and winter cyclone (dashed) packet peak  
481 ( $\text{m s}^{-1}$ ) as a function of lag (h) for the (a) western Pacific and (b) Atlantic  
482 Basins. The gray lines indicate the amplitude normalized by the climatological  
483 standard deviation in meridional wind at that location and date. 25
- 484 5 Zonal group speed ( $\text{m s}^{-1}$ ) as a function of lag (h) for ET (solid) and winter  
485 cyclone (dashed) wave-packet peak in the (a) western Pacific and (b) Atlantic  
486 basins. 26
- 487 6 Wavelength (km) of the ET (solid) and winter cyclone (dashed) wave packet  
488 as a function of lag (h) in the (a) western Pacific and (b) Atlantic basins. 27

489	7	Ensemble-mean meridional temperature flux at $t=0$ for the ET (left column)	
490		and winter cyclone (right column) at 900 hPa (shading, $\text{K m s}^{-1}$ ). The heavy	
491		lines denote the ensemble-mean 900 hPa geopotential height every 20 m, with	
492		negative values dashed. The underlying map in the left column is oriented	
493		such that the composite center longitude at $t=0$ matches the winter cyclone	
494		longitude at $t=0$ .	28
495	8	As in Fig. 7, but for the meridional flux of 900 hPa water vapor mixing ratio	
496		( $\text{g kg}^{-1} \text{ m s}^{-1}$ ).	29
497	9	As in Fig. 2, but for the Atlantic Basin.	30

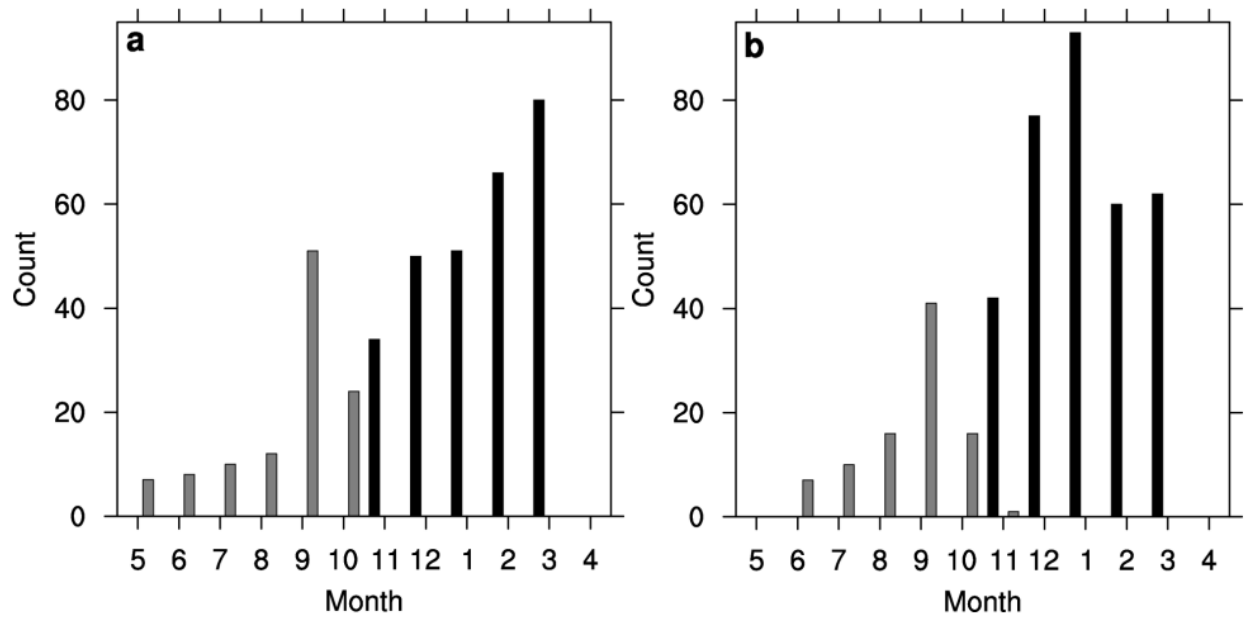


FIG. 1. Number of winter baroclinic cyclone (black) and extratropical transition cases (gray) in the (a) western Pacific and (b) Atlantic basin used in this study as a function of month.

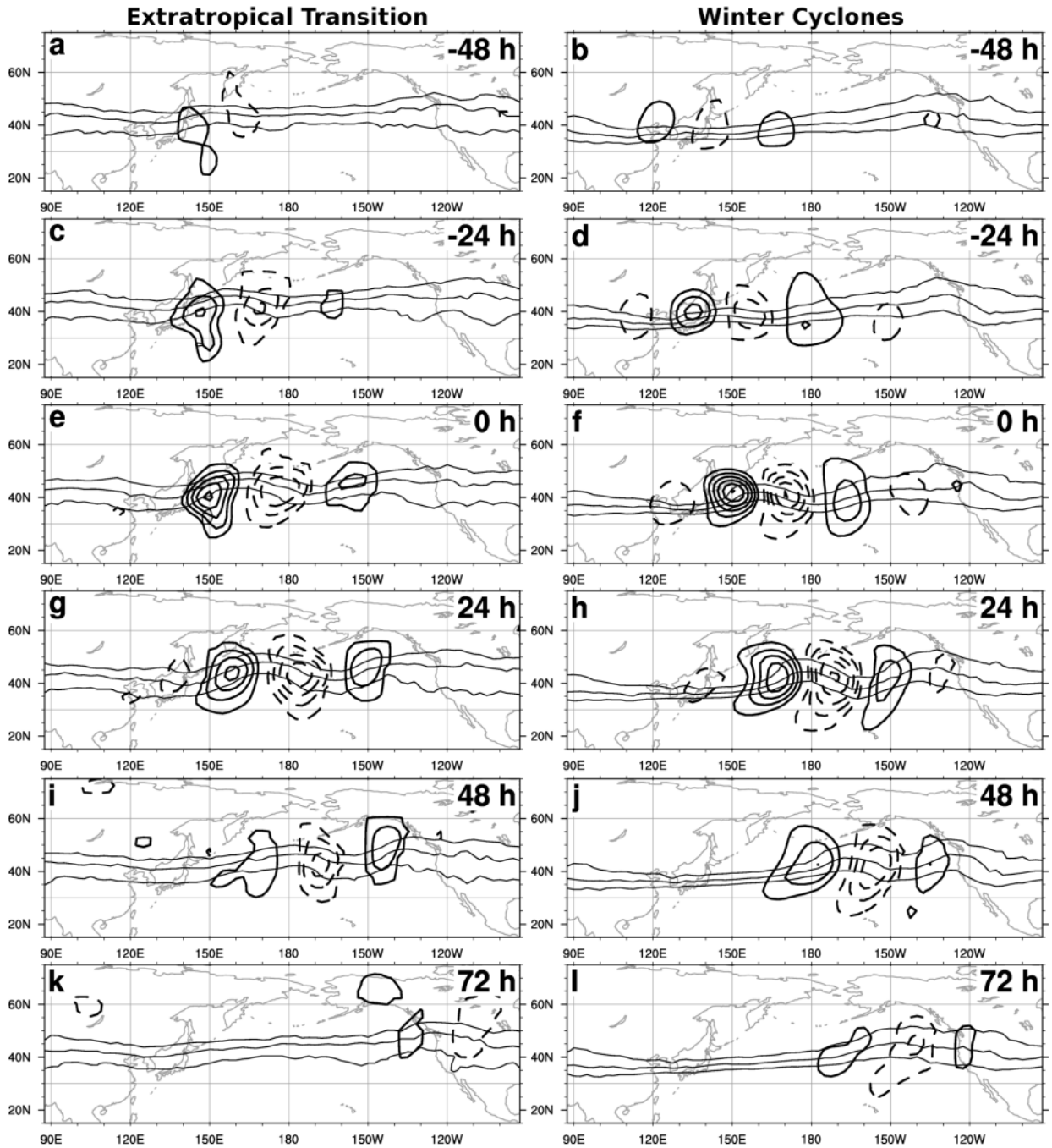


FIG. 2. Ensemble-mean time evolution of the Western Pacific extratropical transition (left column) and winter cyclone (right column) wave packets at 300 hPa. The heavy lines denote the meridional wind every  $3 \text{ m s}^{-1}$ , with dashed indicating negative values, with the zero contour removed. In the left (right) columns, the thin lines denote the 330 K potential vorticity between 3-5 (1-3) PVU [ $1 \text{ PVU} = 10^{-6} \text{ m}^2 \text{ K} (\text{kg s})^{-1}$ ] each 1 PVU. The underlying map in the left column is oriented such that the composite center longitude at  $t=0$  matches the winter cyclone box longitude.

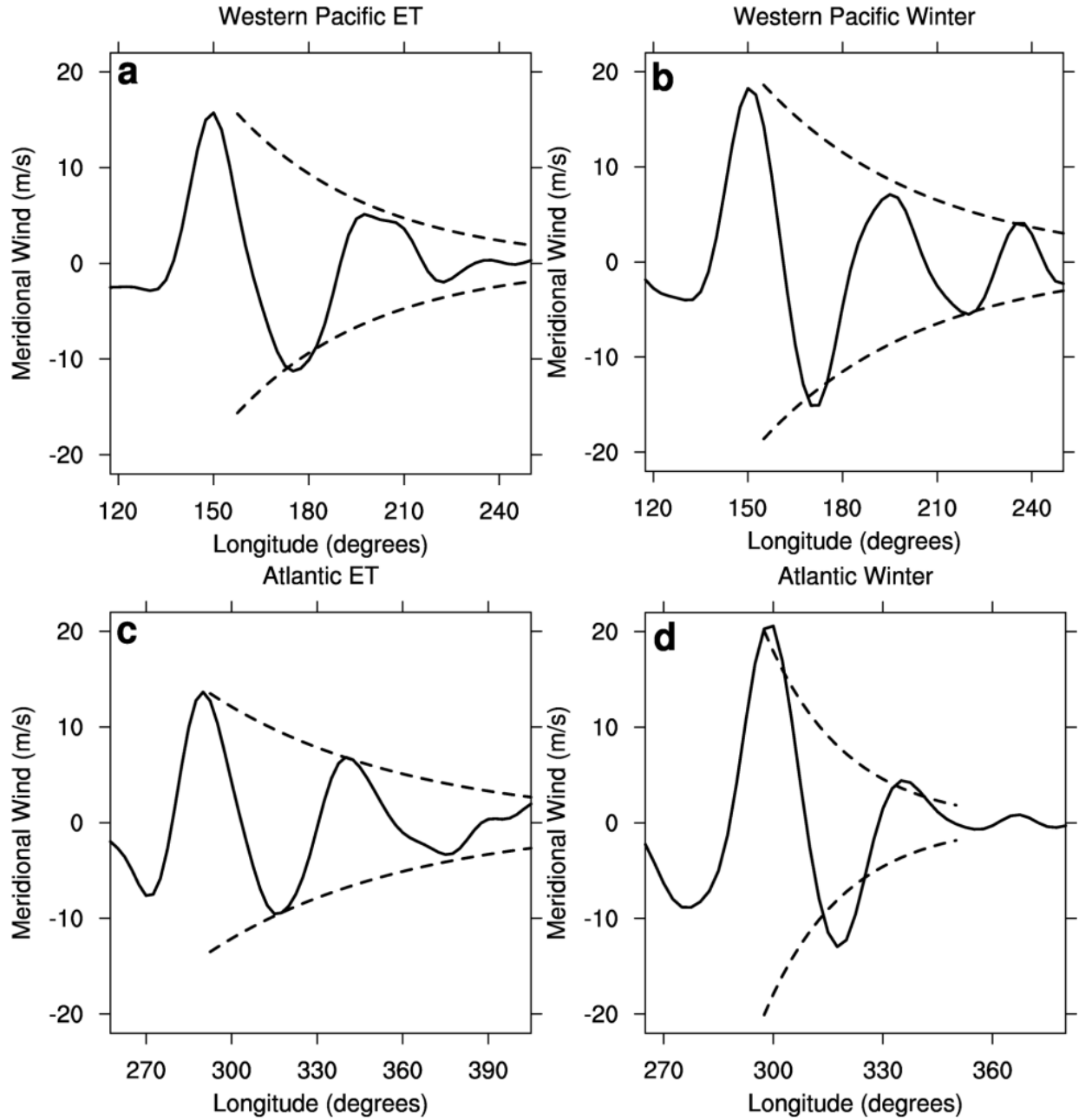


FIG. 3. Western Pacific (a) ET and (b) winter cyclone wave-packet analysis at  $t=0$ . Solid lines denote the anomaly meridional wind ( $\text{m s}^{-1}$ ) as a function of longitude, while the dashed lines are a linear fit to an exponential profile from the packet peak to  $2.5 e$ -folding distances from the peak. (c) and (d) as in (a) and (b) but for Atlantic wave packets.

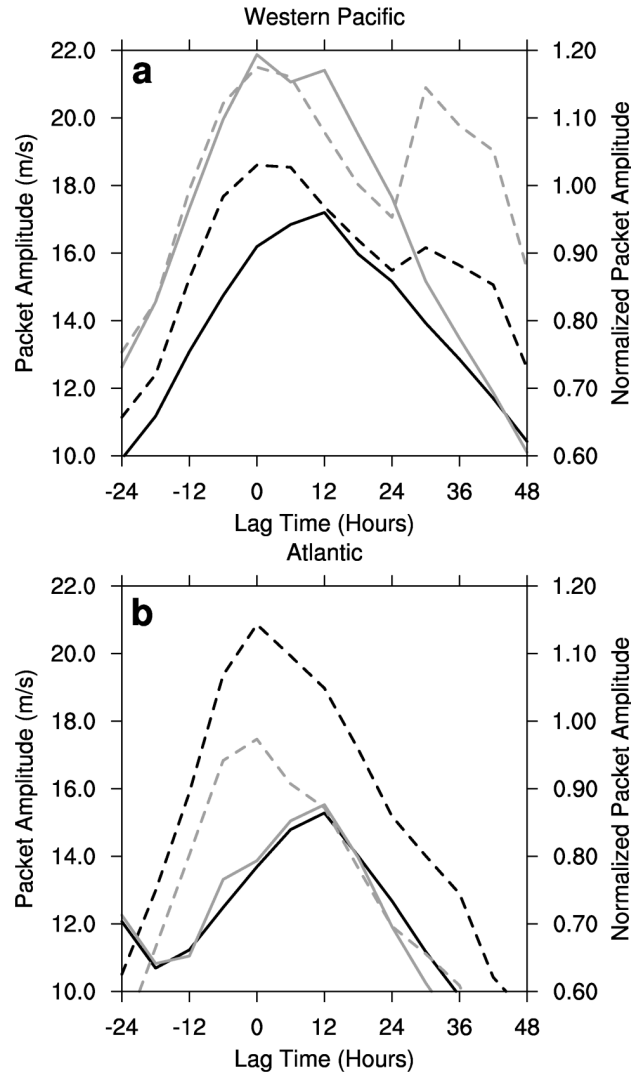


FIG. 4. Amplitude ( $\text{m s}^{-1}$ ) of the ET (solid) and winter cyclone (dashed) packet peak ( $\text{m s}^{-1}$ ) as a function of lag (h) for the (a) western Pacific and (b) Atlantic Basins. The gray lines indicate the amplitude normalized by the climatological standard deviation in meridional wind at that location and date.

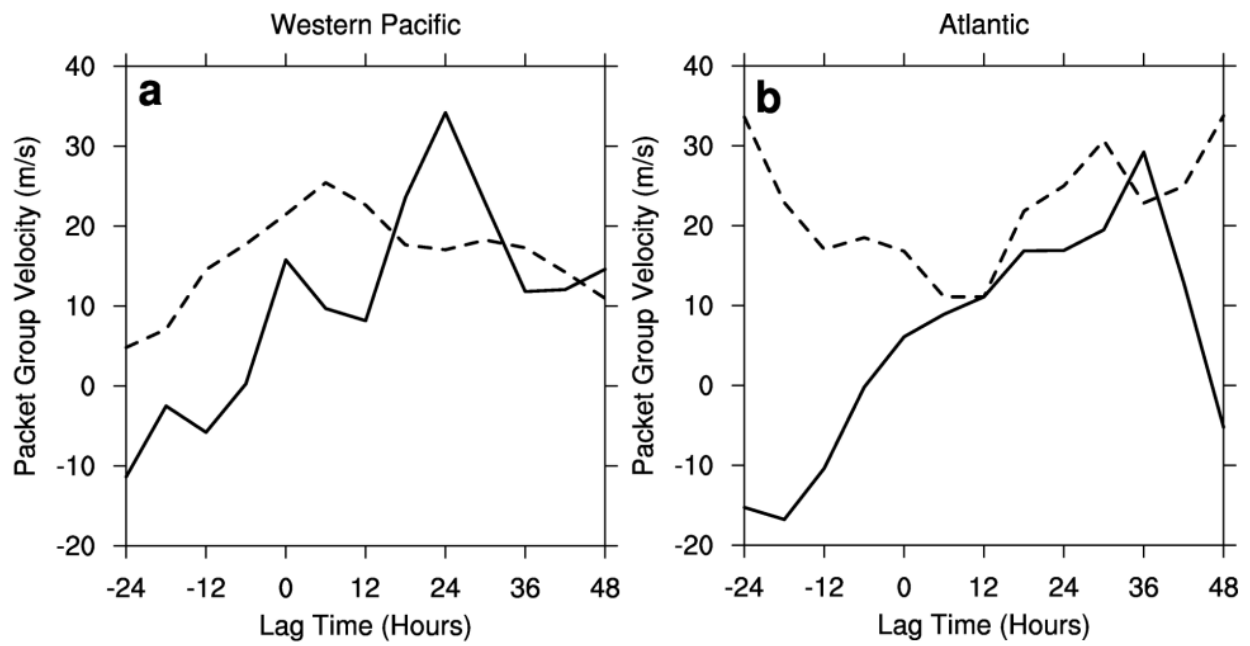


FIG. 5. Zonal group speed ( $\text{m s}^{-1}$ ) as a function of lag (h) for ET (solid) and winter cyclone (dashed) wave-packet peak in the (a) western Pacific and (b) Atlantic basins.

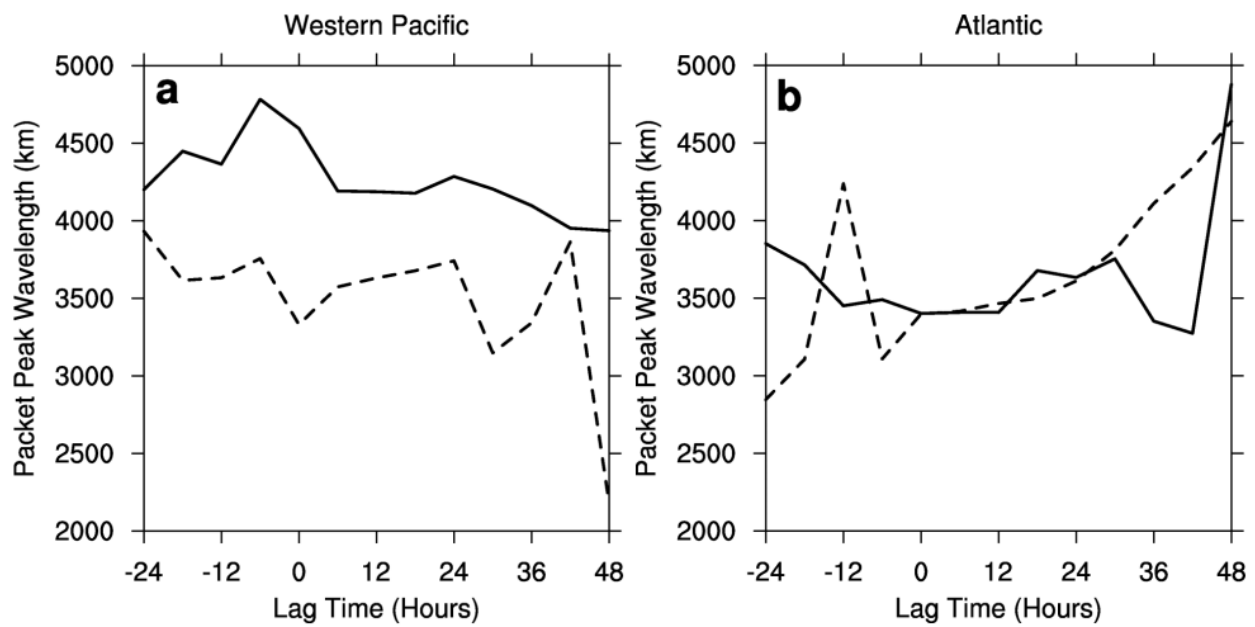


FIG. 6. Wavelength (km) of the ET (solid) and winter cyclone (dashed) wave packet as a function of lag (h) in the (a) western Pacific and (b) Atlantic basins.

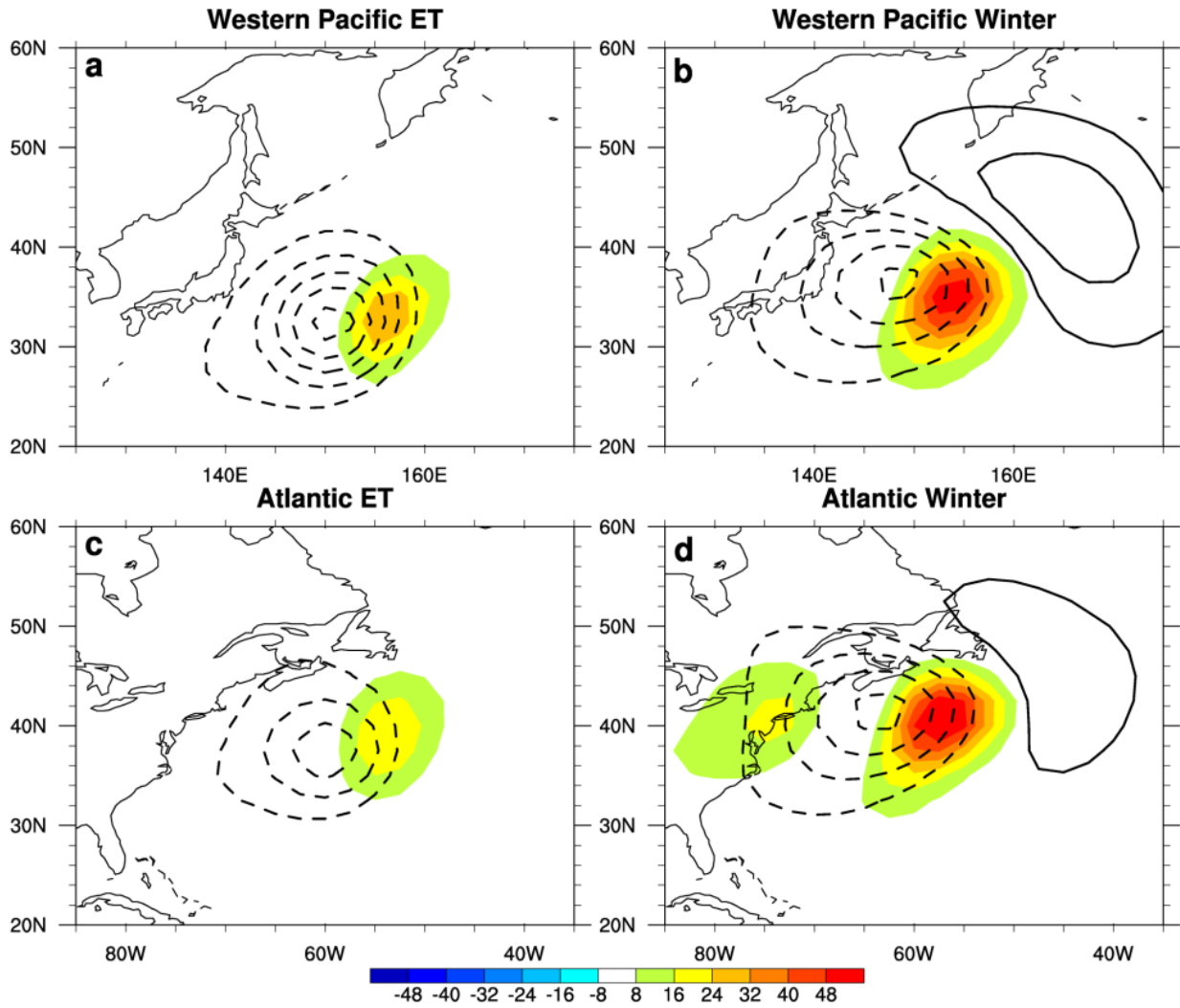


FIG. 7. Ensemble-mean meridional temperature flux at  $t=0$  for the ET (left column) and winter cyclone (right column) at 900 hPa (shading,  $\text{K m s}^{-1}$ ). The heavy lines denote the ensemble-mean 900 hPa geopotential height every 20 m, with negative values dashed. The underlying map in the left column is oriented such that the composite center longitude at  $t=0$  matches the winter cyclone longitude at  $t=0$ .

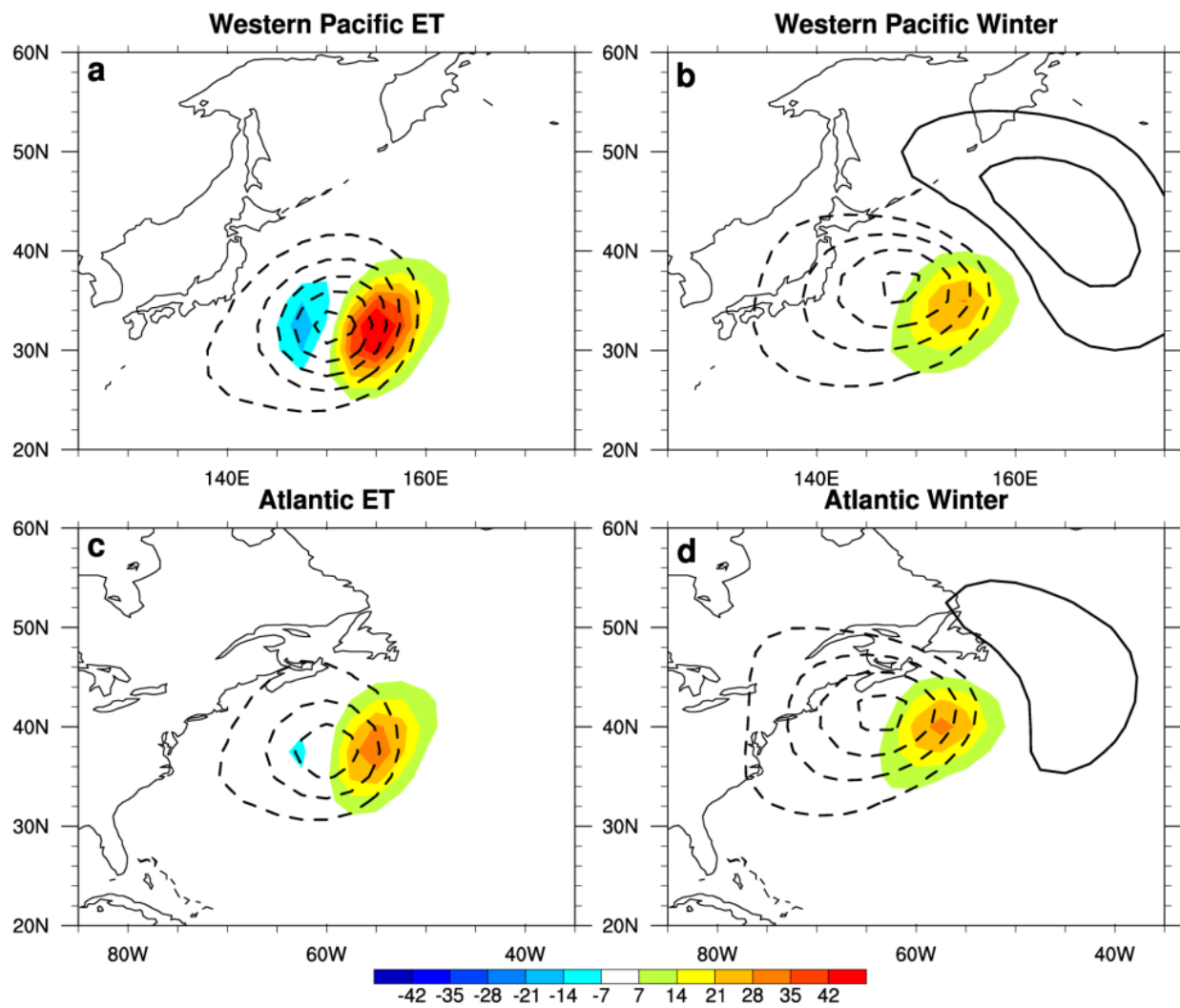


FIG. 8. As in Fig. 7, but for the meridional flux of 900 hPa water vapor mixing ratio ( $\text{g kg}^{-1} \text{m s}^{-1}$ ).

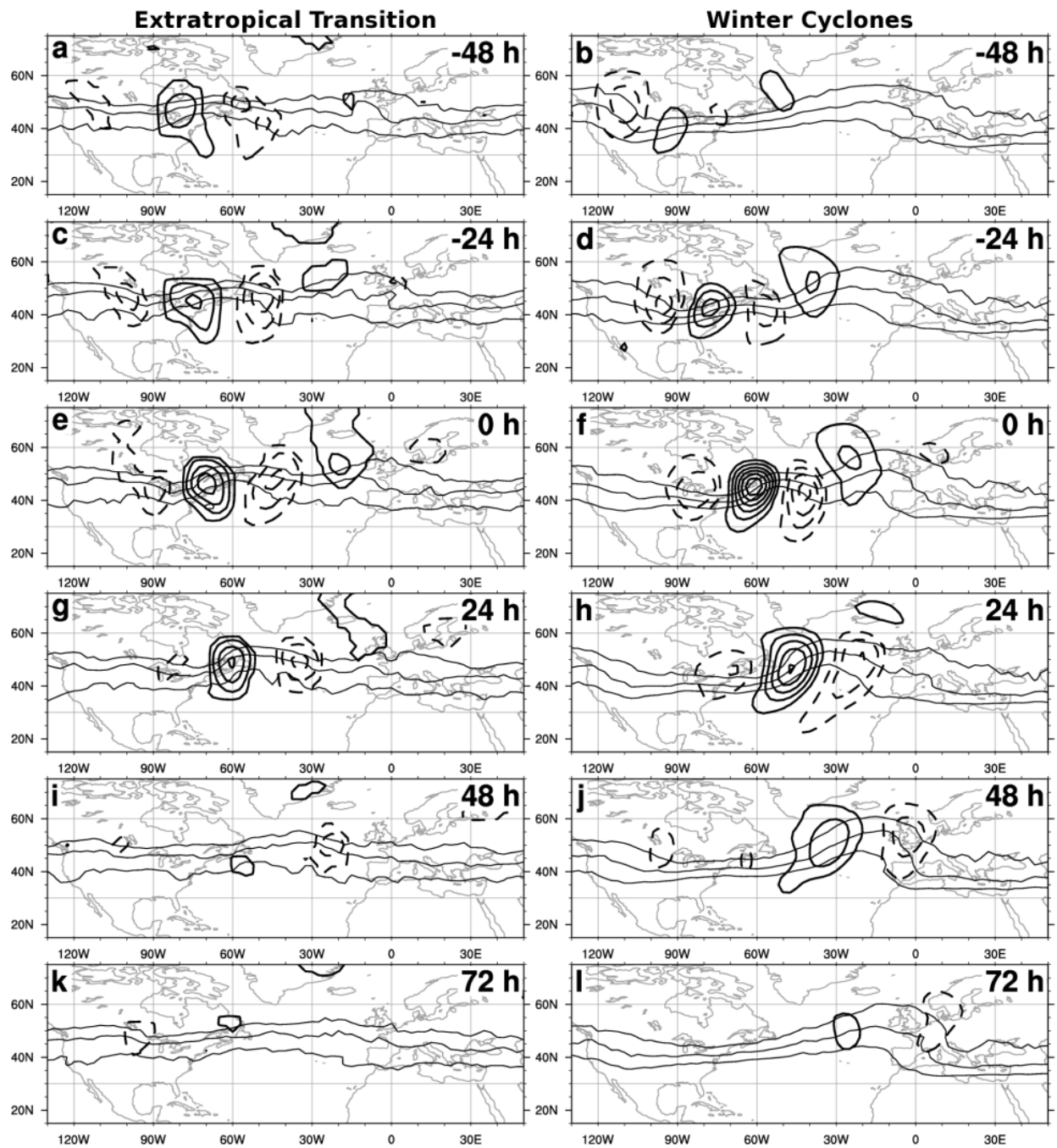


FIG. 9. As in Fig. 2, but for the Atlantic Basin.